Research Square

Preprints are preliminary reports that have not undergone peer review.
They should not be considered conclusive, used to inform clinical practice,
or referenced by the media as validated information.

Selection of a High-Affinity Nitrofurantoin-Specific Aptamer via GO-SELEX and Development of a Fluorescent Aptasensor for Environmental Water Monitoring

Yuzhuo Chen
Chongqing Normal University
Mingdong Cao
Chongqing Normal University
Shuang Jiang
Chongqing Normal University
Yaning Liang
Chongqing Normal University
Yongkang Zhang
Chongqing Normal University
Yujia Xie
Chongqing Normal University
Xuelan Shu
Chongqing Normal University
Dapeng Peng
Zhejiang University
Tao Le
letao@cqnu.edu.cn

Chongqing Normal University

Research Article

Keywords: Nitrofurantoin, GO-SELEX, Aptamer, Molecular simulation, Aptasensor

Posted Date: May 7th, 2026

DOI: https://doi.org/10.21203/rs.3.rs-9174718/v1

License: This work is licensed under a Creative Commons Attribution 4.0 International License.
Read Full License

Additional Declarations: No competing interests reported.

Abstract

Rapid and convenient detection of nitrofurantoin (NFT) residues is critical for ensuring food safety and environmental health, given that its toxic metabolites contribute to ecological damage and the spread of antimicrobial resistance. In this study, we report the first identification of an aptamer specifically targeting NFT using the graphene oxide-based systematic evolution of ligands by exponential enrichment (GO-SELEX). Among the screened candidates, the aptamer AP3 (90 nucleotides) was identified as the optimal probe on the basis of molecular docking, molecular dynamics simulations, and binding free energy analyses and exhibited a high binding affinity, with a dissociation constant (Kd) of 123 nM. Leveraging this aptamer, we developed a novel aptasensor by integrating AP3 with graphene oxide for NFT detection. The aptasensor demonstrated a linear detection range of 20–100 ng/mL and a limit of detection of 10.09 ng/mL. When applied to environmental water samples, the sensor achieved satisfactory recoveries ranging from 94.84% to 112.06%, with coefficients of variation between 4.85% and 14.35%. These findings highlight the potential of the proposed aptasensor as a reliable and effective tool for monitoring NFT residues in complex environmental matrices.

Introduction

Environmental pollution is currently a major concern, and antibiotics can contaminate groundwater and the environment, significantly affecting human health and aquatic life while contributing to antibiotic pollution. Studies have also shown that antibiotics are difficult to degrade and can have detrimental effects on the environment. Nitrofurantoin (NFT) belongs to the nitrofuran class of broad-spectrum antibiotics[1]. Owing to its low cost and strong antimicrobial activity, it has been widely used to treat microbial, bacterial, and protozoan infections in veterinary medicine and farm animals. The use of such substances has been restricted or banned because of their carcinogenic effects*[2]*. However, NFT exhibits pronounced environmental persistence, resistance to natural degradation and transformation into highly cytotoxic species (e.g., nitro anions, nitroso compounds, and hydroxylamine derivatives)[3], thereby posing risks to ecosystems and nontarget organisms[4]. Studies have shown that NFT and its toxic metabolites can attack intracellular macromolecules, resulting in physiological damage and adverse ecological effects even at low concentrations[5]. In addition, the discharge of pharmaceutical wastewater containing NFT may promote the development of antimicrobial resistance in microorganisms, further intensifying public health concerns[6]. Therefore, the detection and monitoring of NFT residues in environmental samples are essential for ensuring ecological safety and protecting human health[7].

Current NFT detection methods primarily target its metabolites and rely on techniques such as ultrahigh-performance liquid chromatography, high-performance liquid chromatography–mass spectrometry, and enzyme-linked immunosorbent assays[8,9]. Although these methods provide high analytical precision, they are time-consuming, require costly instrumentation, involve complex operational procedures, and necessitate skilled personnel. These limitations restrict their application to well-equipped central

laboratories, thereby hindering rapid, onsite analysis in resource-limited settings. Therefore, the development of a sensitive and convenient detection strategy for NFT is imperative[10].

Aptamers, first reported in 1990, are single-stranded DNA or RNA oligonucleotides selected through the systematic evolution of ligands by SELEX. Often termed “chemical antibodies,” they undergo conformational changes to form specific three-dimensional structures upon binding to their targets through hydrogen bonding, electrostatic interactions, and base stacking[11-14]. Aptamers possess several advantages, including diverse target recognition, low cost, ease of synthesis and modification, and high stability[15,16]. To date, numerous aptamers targeting antibiotics[17], toxins[18], proteins[19], and heavy metal ions[20] have been developed for analytical applications. These aptamers are widely employed in various sensing platforms, such as fluorescence[21], electrochemical[22], and lateral flow assays[23]. Among these, fluorescence-based aptasensors are particularly favorable because of their versatility, sensitivity, and operational simplicity[24,25]. In fluorescent aptasensors utilizing nanomaterials (e.g., quantum dots[26], gold nanoparticles[27], and silicon nanoparticles[28]), GO is typically used as a fluorescent probe carrier because of its abundant functional groups, large specific surface area, and strong fluorescence quenching ability[29]. In such systems, fluorophore-labeled aptamers adsorb onto GO via electrostatic and π–π interactions, resulting in quenched fluorescence. Upon target binding, the aptamer detaches from the GO surface, leading to fluorescence recovery, which is correlated with the target concentration[30]. This mechanism is particularly effective for small-molecule detection.

Here, we employed GO-SELEX to screen high-affinity aptamers against NFT. Secondary structure prediction (NUPACK), molecular docking (AutoDock Vina), and MD were applied to identify optimal sequences and elucidate their binding mechanisms. On the basis of the selected aptamer, a simple yet efficient fluorescent aptasensor was subsequently developed for accurate NFT detection in environmental samples.

Materials and Methods

Materials and reagents

Nitrofurantoin (NFT), nitrofurazone (NFZ), furazolidone (FZD), furaltadone (FTD), and 1-aminohydantoin (AHD) were purchased from Shanghai Aladdin Biochemical Technology Co., Ltd. (China). Streptavidin magnetic beads were obtained from Promega Corporation. GO was obtained from Nanjing XFNANO Technology Co., Ltd. (China). All other chemicals, including $MgCl_2$, NaCl, KCl, and 10×TBE buffer, were of analytical grade and supplied by Sangon Biotech Co., Ltd. (Shanghai, China). Oligonucleotides were synthesized by Sangon Biotech Co., Ltd. (Table S1).

Preparation of the GO and Library

A 2 mg/mL GO dispersion (1 mL) was centrifuged at 15,000 rpm (25°C) for 10 min, after which the supernatant was discarded. The pellet was resuspended in 1 mL of binding buffer I (20 mM Tris, 100 mM NaCl, 5 mM KCl, 2 mM $MgCl_2$, and 1 mM $CaCl_2$; pH 7.4), vortexed, and centrifuged under identical conditions. This washing step was repeated three times. The final pellet was dispersed in 1 mL of binding buffer I, sonicated, and stored at 4°C. The ssDNA library and primers were dissolved in binding buffer I, denatured at 95°C for 10 min, rapidly cooled on ice for 10 min, and equilibrated at room temperature for 10 min. The library and primers were diluted to 500 nM and stored at -20°C.

In Vitro Selection of Aptamers

The GO-SELEX procedure is illustrated in Fig. 1. Briefly, 200 μL of activated ssDNA library (500 nM) was mixed with 20 μL of NFT solution (10 μg/mL in acetonitrile diluted with binding buffer I) and incubated at 25°C for 1 h. The ssDNA-NFT complexes were separated from unbound ssDNA by the addition of GO, which adsorbed free ssDNA via π–π stacking and electrostatic interactions. After centrifugation (15,000 rpm, 10 min), the supernatant was PCR-amplified. The PCR product was incubated with streptavidin magnetic beads, washed with PBS, and eluted with 0.05 M NaOH. The eluent was neutralized with 0.05 M HCl, adjusted with binding buffer II (40 mM Tris, 180 mM NaCl, 10 mM KCl, 4 mM $MgCl_2$, 2 mM $CaCl_2$; pH 7.4), and magnetically separated to obtain the enriched library.

Counterselections against structural analogs (NFZ, FTD, FZD, AHD, SEM, AMOZ, and AOZ) were performed to eliminate nonspecific sequences. After stable enrichment was reached, the final library was cloned and sequenced.

Secondary Structure Prediction and Molecular Docking

After screening, the aptamer sequences were cloned and sequenced by Sangon Biotech (Shanghai) Co., Ltd. The sequences were aligned and analyzed for homology and phylogenetic trees using DNAMAN software (Lynnon Biosoft, USA). On the basis of sequence homology, the sequences were divided into families. To simulate actual experimental conditions (including temperature and ion concentration), the secondary structures of the family members were predicted using the NUPACK platform (https://nupack.org), and the candidate sequences with the lowest free energy (ΔG) in each family were selected for further study[31]. The three-dimensional structures of the candidate aptamers were modeled using the 3dRNA/DNA online tool[33] (http://biophy.hust.edu.cn/). The molecular structures of NFT and its analogs were obtained from the PubChem database (https://pubchem.ncbi.nlm.nih.gov/), and the Multiwfn program and ORCA program[34] were employed in conjunction to optimize the molecular geometry and perform RESP2 electrostatic potential fitting alongside structural optimization. MD between the candidate aptamers and NFT and its analogs was performed using AutoDock Vina (version 1.2.5). The sequences with the highest specificity were selected on the basis of the binding Gibbs free energy, and MD was performed to verify the binding stability.

Affinity and specificity analysis

A control experiment was designed to analyze the affinity and specificity of the aptamers. In the affinity evaluation system, the experimental groups were treated with gradient concentrations (12.5, 25, 50, 100, and 200 nM) of the candidate aptamer solution (200 μL) and 10 μL of the NFT standard (1 μg/mL), incubated in the dark, and then treated with a precisely calculated mass-matched GO solution for 10 minutes. The control group was treated with an equal volume of buffer instead of the NFT standard. After centrifugation at 15,000 rpm for 10 minutes, the fluorescence intensity of the supernatant was measured using a fluorescence spectrophotometer at an excitation wavelength of 492 nm and an emission wavelength of 518 nm. The background fluorescence value (F0) of the control group and the fluorescence value (F) of the experimental group were recorded, and the relative fluorescence intensity (ΔF = F - F0) was calculated.

A nonlinear regression model Y = Mmax × X/(Kd + X)[32] was established, and Origin 8.0 software was used for curve fitting, with the aptamer molar concentration as the independent variable (X-axis) and ΔF as the dependent variable (Y-axis). The dissociation constant (Kd) was calculated, indicating the binding affinity of the aptamer-NFT complex. A lower Kd value indicates stronger binding ability.

In the specificity evaluation experiment, the candidate aptamer concentration was fixed at 100 nM (200 μL), and equal volumes (10 μL) of NFT and its structural analogs (all at a concentration of 1 μg/mL) were coincubated. The above steps were repeated, and ΔF was compared to evaluate the specificity of the candidate aptamers.

MD and binding free energy

GROMACS 2023.3 and gmx_MMPBSA 1.6.2 software were used to simulate the interaction between the selected sequence and NFT [36,37]. The MD of the aptamer candidate sequences in complex with NFT and its metabolites was conducted using the GROMACS software package (version 2023.3), with the key systems simulated for 300 ns. The aptamer was parameterized using the AMBER ff14SB force field with parmbsc1 correction[34,38]. The system was solvated in a cubic box with TIP3P explicit water molecules, ensuring a minimum distance of 1.0 nm between the solute and the box boundaries. To mimic physiological conditions, the system was neutralized with Na^+ and Cl^- ions at a concentration of 0.15 M. The equilibration procedure involved three consecutive steps: initial energy minimization, followed by stabilization under constant volume and temperature conditions, and finally equilibration under constant pressure and temperature conditions.

Production simulations were conducted under NPT ensemble conditions using the V-rescale thermostat[39] and C-rescale barostat for temperature and pressure control[40], respectively. Long-range electrostatic interactions were computed using the particle–mesh Ewald method, whereas hydrogen-involved bonds were constrained with the LINCS algorithm. The simulations utilized an integration time

step of 2.0 fs, with trajectory data sampled every 5,000 steps. This sampling scheme yielded 30,000 frames (300 ns) per system for subsequent analysis.

Binding free energy calculations were performed using the gmx_MMPBSA tool on MD trajectories. The MM/GBSA method with the GB-Neck2[41] implicit solvent model was applied, maintaining an ion concentration of 0.15 M and consistent parameters with those of the MD simulations. Per-nucleotide decomposition analysis was conducted to evaluate the contribution of individual residues to the overall binding affinity.

Optimization of the Aptamer

To improve the sensitivity and convenience of the aptamer-based fluorescent sensor, the GO concentration, aptamer concentration, buffer type, pH, incubation time, and quenching time were optimized. FAM-AP3 (100 nM) was incubated with different concentrations of GO (0, 100, 150, 200, 250, 300 μg/mL) to determine the optimal GO concentration for quenching. At the optimal GO concentration, the FAM-AP3 concentration was optimized by incubating different concentrations of the aptamer (50, 100, 150, 200, 250 nM) with 10 μL of NFT (1 μg/mL) in the dark, followed by the addition of the optimized GO concentration. The control group had no target, and the relative fluorescence intensity was calculated. FAM-AP3 and NFT were incubated in different buffer systems (HEPES, binding buffer, H_2O, and PBS), and GO was added to measure the relative fluorescence intensity. Buffers with different pH values (6.4, 6.9, 7.4, 7.9, and 8.4) were used to measure the relative fluorescence intensity. Finally, different incubation times (10, 20, 30, 40, and 50 minutes) and quenching times (0, 2, 4, 6, 8, and 10 minutes) were adjusted to determine the optimal incubation and quenching times for the aptasensor.

Aptasensor detection performance

The detection procedure was conducted in a 200 μL reaction system containing 100 μL of FAM-AP3 (400 nM) mixed with NFT solutions at varying final concentrations (15, 20, 40, 60, 80, 100, 150, and 200 ng/mL). The mixtures were incubated at 25°C in the dark for 30 min, followed by the addition of GO (250 μg/mL) and further incubation in the dark for 8 min. Subsequently, the solutions were centrifuged at 15,000 rpm for 10 min, after which the fluorescence of the supernatant was measured. A control group without the target was included, and a standard curve for NFT quantification was established using relative fluorescence intensity. The LOD was calculated as 3 SD/slope, where SD represents the standard deviation of the fluorescence intensity from that of the blank samples, and the slope was derived from the linear regression curve. To evaluate the specificity of the aptasensor, FAM-AP3 was incubated with 1 μg/mL NFT or its structural analogs under identical conditions, and the relative fluorescence intensities were compared to assess cross-reactivity.

Real Sample Analysis

Water and soil samples were collected from aquaculture and residential areas and processed according to the instructions in the supplementary material. After the absence of NFT in the samples was confirmed using HPLC, different concentrations of NFT (30, 60, and 90 ng/mL) were added, and the aptasensor was used for detection. The results were compared with those obtained by HPLC to verify the reliability of the aptasensor. The recovery rate was calculated as (measured concentration/known concentration) × 100%, and the coefficient of variation was determined. Each spiked sample was analyzed five times.

Results and Discussion

Screening of NFT Aptamer

In the GO-SELEX-based screening, sequences not bound to NFT were efficiently adsorbed onto the GO surface through π–π stacking, enabling rapid separation of target-bound sequences. The high screening efficiency of GO is attributed to its surface-rich oxygen-containing functional groups (such as hydroxyl and carboxyl groups), large specific surface area, and excellent water dispersibility, which significantly increase the interaction between the nucleic acid library and GO. Moreover, the nonimmobilized target format avoids the impact of target immobilization on conformation, further improving screening efficiency. The screening process (Fig. S1) revealed that the aptamer enrichment efficiency steadily increased and stabilized by the 7th round. In the 8th round, structural analogs of NFT were introduced for counterscreening, and the recovery rate of specific sequences decreased sharply to 11%, indicating the effective removal of nonspecific binding sequences. The final screening round was subsequently conducted, and the recovery rate rebounded to 58%, suggesting the successful enrichment of high-affinity aptamers. After screening, the 9th round product was cloned and sequenced, yielding 47 candidate sequences.

Secondary Structure and Molecular Docking Analysis

On the basis of sequence homology-guided cluster analysis, the 47 candidate aptamers obtained through screening were classified into 13 distinct families. The folding free energy of each individual aptamer was determined and is listed to evaluate the secondary structural stability of representative sequences from each family (Table S5). Lower minimum free energy values (e.g., AP3: -17.49 kcal/mol) indicated higher conformational stability in the predicted secondary structures, which is advantageous for maintaining the functional activity of the aptamers in solution. The most stable sequence from each family was selected and designated AP1 through AP13. MD was subsequently performed to screen candidate sequences through comprehensive analysis of their binding free energies with NFT and its structural analogs.

Five sequences (AP2, AP3, AP6, AP12, and AP13) were selected for affinity determination. The docking scores revealed that these five sequences strongly interacted with NFT (binding free energy < -7.5 kcal/mol) but showed negligible cross-reactivity with structural analogs (Fig. S3**)**. Although AP1 displayed tight binding to NFT, it was excluded because of its interactions with other structural analogs.

Screening of Optimal Aptamer Candidates by Molecular Docking and MD Simulations

In this study, five aptamers (AP2, AP3, AP6, AP12, and AP13) prescreened by molecular docking were selected as receptors, and NFT was used as the ligand for MD simulations and binding free energy calculations. The stability of each aptamer-NFT complex and the strength of their intermolecular interactions were evaluated on the basis of root-mean-square deviation (RMSD) and hydrogen bond analyses.

The RMSD profiles of the AP2-NFT, AP3-NFT, AP6-NFT, AP12-NFT, and AP13-NFT complexes are shown in Fig. 2A–E, with average RMSD values of 2.401 nm, 1.702 nm, 2.951 nm, 2.741 nm, and 2.659 nm, respectively. Among them, the AP3-NFT complex has the lowest average RMSD, indicating the smallest structural deviation and the highest overall stability. As shown in Fig. 2B**,** the RMSD of AP3 becomes highly stable after 100 ns and remains close to 1.702 nm, suggesting that the complex reaches dynamic equilibrium. In contrast, most other aptamer systems fail to reach a stable equilibrium state, except for AP12, whose RMSD begins to converge after 50 ns.

Further conformational analyses confirmed these findings. AP3 maintained a relatively stable conformation throughout the 60–300 ns simulation (Fig. 3B), whereas AP6 underwent substantial structural fluctuations and failed to maintain stable binding (Fig. 3C). Similar conformational instability was observed for AP2, AP12, and AP13 (Fig. 3A, 3D, 3E). Overall, AP3 displays the most favorable stability, followed by AP12.

Hydrogen bonding is an essential driving force for nucleic acid aptamer recognition of target molecules. The number of hydrogen bonds formed between each aptamer and NFT over the course of the simulation is presented in Fig.s 2F–2J, with average values of 0.947, 1.481, 3.750, 0.766, and 0.712 for AP2, AP3, AP6, AP12, and AP13, respectively. Although AP6 forms the greatest number of hydrogen bonds and AP3 ranks second, these results are not fully consistent with those of the RMSD-based stability analysis. This discrepancy suggests that aptamer—ligand interactions are governed not only by hydrogen bonding but also by hydrophobic forces, π—π stacking, and other noncovalent interactions; therefore, hydrogen bonding cannot be used as the sole evaluation criterion.

To further quantify binding affinity, MM/GBSA binding free energy calculations were performed. As shown in Fig. 2K-2O, all the aptamers exhibit varying degrees of interaction with NFT, with average binding free energies of −10.422 kcal/mol, −13.773 kcal/mol, −13.801 kcal/mol, −9.403 kcal/mol, and −9.359 kcal/mol for AP2, AP3, AP6, AP12, and AP13, respectively. These results indicate that AP3 and AP6 have the strongest binding affinity for NFT. Decomposition of binding free energy into different energetic components (Fig.s 2P-2T) reveals that van der Waals forces dominate the favorable contributions to binding, whereas electrostatic interactions are unfavorable. This confirms that the aptamer–NFT interaction is driven primarily by hydrogen bonding, hydrophobic effects, and π-stacking interactions.

Taken together, the combined MD stability evaluation, hydrogen bonding analysis, and binding free energy calculations identify AP3 and AP6 as the most promising NFT-binding aptamers, with AP3 displaying slightly superior structural stability. On the basis of these computational results, AP3 was predicted to be the optimal candidate for subsequent experimental verification of its affinity and specificity.

Aptamer affinity and specificity analysis

Following the computational screening, the five candidate sequences (AP2, AP3, AP6, AP12, and AP13) were experimentally characterized. First, their binding with NFT was measured using a GO-based fluorescence quenching assay. The resulting dose—response data were subsequently processed using a nonlinear regression equation in Origin 2021 software (Northampton, MA) to calculate the respective Kd (Fig. 4A).

The Kd values of these sequences ranged from 123 to 330 nM, demonstrating their high affinity for NFT. Among them, AP6 exhibited a Kd of 140 nM, while AP3 displayed the strongest binding, with a Kd of 123 nM. Comparative analysis of cross-binding with structural analogs revealed that AP3 exhibited superior selectivity (Fig.s 4B-4F), which led to its selection as a detection probe for the aptasensor. The experimental results for affinity and specificity conclusively validated the computational predictions, confirming that AP3 is indeed the best-performing aptamer. The underlying mechanism responsible for the high affinity and selectivity between NFT and these sequences was elucidated by the preceding MD, which investigated the binding interactions between the sequences and NFT.

Optimization of Aptasensor Conditions

The detection principle of the GO-based aptamer fluorescence sensor is illustrated in Fig. 5A, where the sensing performance depends on the system components. Optimal fluorescence recovery was achieved at a GO concentration of 250 μg/mL (Fig. 5B) and a FAM-AP3 concentration of 200 nM (Fig. 5C), which balanced sensitivity (by avoiding excessive adsorption) and cost efficiency (by minimizing aptamer waste). Bonding buffer at pH 7.4 yielded the highest relative fluorescence intensity (Fig. 5D, Fig. 5E). The optimal incubation time for NFT and FAM-AP3 was determined to be 30 min (Fig. 5F), while the quenching time for the complex with GO was 8 min (Fig. 5H). These conditions ensured high detection sensitivity, reduced fabrication costs, and shortened the duration of the assay. Consequently, the aptasensor was constructed using GO (250 μg/mL), FAM-AP3 (200 nM), and pH 7.4 binding buffer, with incubation and quenching times of 30 min and 8 min, respectively.

Analysis of the Detection Performance of the Aptasensor

Under optimized experimental conditions, the fluorescence intensity of the aptasensor exhibited an optimal linear relationship with NFT concentrations ranging from 20~100 ng/mL. The linear regression equation was $Y = 0.02113X + 0.09965$ ($R^2 = 0.9907$), with an LOD of 10.09 ng/mL for NFT. This sensitivity is suitable for routine monitoring and, crucially, is achieved without the need for complex noble metal or

nanomaterial modifications often required in electrochemical sensors. Cross-reactivity tests with structural analogs revealed that the aptamer sensor generated strong fluorescence signals in the presence of NFT, whereas responses to other structural analogs exhibited fluorescence intensities below 20%. This exceptional specificity, inherent to the molecular recognition of the aptamer, significantly surpasses that of most electrochemical sensors, which often suffer from interference from structurally similar compounds. Collectively, these results demonstrate the outstanding detection performance of the developed aptasensor, particularly in terms of selectivity and operational simplicity, compared to electrochemistry-based platforms [41].

Validation of Aptamer Detection Performance

The detection capability of the aptasensor was analyzed using spiked samples at different concentrations (30, 60, and 90 ng/mL) to evaluate its applicability in complex environments. The reliability of the aptasensor was further verified by comparing its performance with that of HPLC for the same spiked samples. As shown in Table 2, the aptasensor demonstrated average recoveries ranging from 94.84% to 112.06% and coefficients of variation between 3.77% and 15.25% across the four sample types. These results were positively correlated with the HPLC data, which indicated that the aptasensor reliably detected environmental NFT residues.

Conclusions

In summary, in this study, an anti-NFT aptamer (AP3) was successfully obtained through GO-SELEX screening. A GO-based fluorescence sensor was constructed using FAM-labeled AP3 as the fluorescent probe, achieving a dynamic linear detection range of 20–100 ng/mL and an LOD of 10.09 ng/mL, which demonstrated comparable or superior performance to previously reported methods. Spike recovery tests in four real-world samples yielded recoveries ranging from 94.84%-112.06%, with coefficients of variation ranging from 4.85%-14.35%, indicating excellent recovery and a strong correlation with standard HPLC results. This work establishes an effective aptamer-based tool for NFT detection and provides a conceptual foundation for future environmental antibiotic residue monitoring.

Declarations

Acknowledgements

This work was supported by the Science and Technology Research Program of Chongqing Municipal Education Commission (Grant No. KJZD-M202400501).

Authors' contributions

Y.C.: Writing – review & editing, Data curation, Formal analysis, Software, Methodology, Visualization. M.C.: Writing – original draft, Writing – review & editing, Conceptualization, Data curation, Formal analysis, Methodology, Validation. S.J.: Software, Methodology, Investigation, Visualization. Y.L.: Software, Methodology, Investigation, Formal analysis. Y.Z.: Validation, Investigation, Formal analysis.

Y.X.: Investigation, Formal analysis, Visualization. X.S.: Software, Methodology, Validation. D.P.: Writing – review & editing, Supervision, Resources, Validation. T.L.: Writing – review & editing, Supervision, Project administration, Funding acquisition, Conceptualization, Methodology. All authors read and approved the final manuscript.

Funding
This research did not receive any specific grants from funding agencies from public, commercial, or not-for-profit sectors.

Data availability

Not applicable.

Ethics approval and consent to participate

Not applicable.

Consent for publication

Not applicable.

Competing interests

The authors declare no competing interests.

References

1. Cheng, Z.; Liu, X.F.; Zhao, B.B.; Liu, X.; Yang, X.R.; Zhang, X.Y.; Feng, X. A smartphone-integrated test paper sensing platform for visual and intelligent detection of nitrofurantoin in honey samples. *Food Chemistry* **2024**, *445*.
2. Yang, H.F.; Qin, L.N.; Wen, H.; Ding, M.Y.; Zhang, L.W.; Xiao, J.X.; Liang, J.X.; Liu, Y.T.; Yu, Z.Y.; Peng, D.P. Preparation of high-affinity and high-specificity monoclonal antibody and development of ultrasensitive immunoassay for the detection of 1-amino-hydantoin, the metabolite of nitrofurantoin. *Food Chemistry* **2024**, *456*.
3. Wen, X.; Yan, X.; Zheng, X.; Kou, Q.; Yang, L.; Tang, J.; Chen, X.; Xie, Y.; Le, T. Selection and truncation of aptamers as fluorescence sensing platforms for selective and sensitive detection of nitrofurazone. *Analytica Chimica Acta* **2023**, *1252*.
4. Zhang, Y.; Qiao, H.; Chen, C.; Wang, Z.; Xia, X. Determination of nitrofurans metabolites residues in aquatic products by ultra-performance liquid chromatography–tandem mass spectrometry. *Food Chemistry* **2016**, *192*, 612-617.
5. Wang, Y.; Chan, K.K.J.; Chan, W. Plant uptake and metabolism of nitrofuran antibiotics in spring onion grown in nitrofuran-contaminated soil. *Journal of Agricultural and Food Chemistry* **2017**, *65*, 4255-4261.

6. Pacholak, A.; Zdarta, A.; Frankowski, R.; Cybulski, Z.; Kaczorek, E. Exploring elimination kinetics of four 5-nitrofuran derivatives by microbes present in rural and municipal activated sludge. *Water, Air, & Soil Pollution* **2020**, *231*.
7. Lewkowski, J.; Rogacz, D.; Rychter, P. Hazardous ecotoxicological impact of two commonly used nitrofuran-derived antibacterial drugs: Furazolidone and nitrofurantoin. *Chemosphere* **2019**, *222*, 381-390.
8. Zheng, X.; Xie, Y.; Chen, Z.; Cao, M.; Lei, X.; Le, T. A comprehensive review on the pretreatment and detection methods of nitrofurans and their metabolites in animal-derived food and environmental samples. *Food Chemistry: X* **2024**, *24*.
9. Song, M.; Li, C.; Wu, S.; Duan, N. Screening of specific aptamers against chlorpromazine and construction of novel ratiometric fluorescent aptasensor based on metal-organic framework. *Talanta* **2023**, *252*.
10. Mariyappan, V.; Keerthi, M.; Chen, S.-M.; Jeyapragasam, T. Nanostructured perovskite type gadolinium orthoferrite decorated rgo nanocomposite for the detection of nitrofurantoin in human urine and river water samples. *Journal of Colloid and Interface Science* **2021**, *600*, 537-549.
11. Wang, S.; Liu, J.; Yong, W.; Chen, Q.; Zhang, L.; Dong, Y.; Su, H.; Tan, T. A direct competitive assay-based aptasensor for sensitive determination of tetracycline residue in honey. *Talanta* **2015**, *131*, 562-569.
12. Radom, F.; Jurek, P.M.; Mazurek, M.P.; Otlewski, J.; Jelen, F. Aptamers: Molecules of great potential. *Biotechnol Adv* **2013**, *31*, 1260-1274.
13. Kong, Q.; Yue, F.; Liu, M.; Huang, J.; Yang, F.; Liu, J.; Li, J.; Li, F.; Sun, X.; Guo, Y*., et al.* Nonimmobilized go-selex of aptamers for label-free detection of thiamethoxam in vegetables. *Anal Chim Acta* **2022**, *1202*, 339677.
14. Liu, X.; Gao, T.; Gao, X.; Ma, T.; Tang, Y.; Zhu, L.; Li, J. An aptamer based sulfadimethoxine assay that uses magnetized upconversion nanoparticles. *Microchimica Acta* **2017**, *184*, 3557-3563.
15. Dolati, S.; Ramezani, M.; Nabavinia, M.S.; Soheili, V.; Abnous, K.; Taghdisi, S.M. Selection of specific aptamer against enrofloxacin and fabrication of graphene oxide based label-free fluorescence assay. *Anal Biochem* **2018**, *549*, 124-129.
16. Chakraborty, B.; Das, S.; Gupta, A.; Xiong, Y.; T-V, V.; Kizer, M.E.; Duan, J.; Chandrasekaran, A.R.; Wang, X. Aptamers for viral detection and inhibition. *ACS Infect Dis* **2022**, *8*, 667-692.
17. Chinnappan, R.; Eissa, S.; Alotaibi, A.; Siddiqua, A.; Alsager, O.A.; Zourob, M. In vitro selection of DNA aptamers and their integration in a competitive voltammetric biosensor for azlocillin determination in waste water. *Analytica Chimica Acta* **2020**, *1101*, 149-156.
18. Li, Z.; Hu, B.; Zhou, R.; Zhang, X.; Wang, R.; Gao, Y.; Sun, M.; Jiao, B.; Wang, L. Selection and application of aptamers with high-affinity and high-specificity against dinophysistoxin-1. *RSC Advances* **2020**, *10*, 8181-8189.
19. Thelu, H.V.P.; Atchimnaidu, S.; Perumal, D.; Harikrishnan, K.S.; Vijayan, S.; Varghese, R. Self-assembly of an aptamer-decorated, DNA–protein hybrid nanogel: A biocompatible nanocarrier for targeted

cancer therapy. *ACS Applied Bio Materials* **2019**, *2*, 5227-5234.

20. Feng, D.; Li, P.; Tan, X.; Wu, Y.; Wei, F.; Du, F.; Ai, C.; Luo, Y.; Chen, Q.; Han, H. Electrochemiluminescence aptasensor for multiple determination of hg^{2+} and pb^{2+} ions by using the mil-53(al)@cdte-pei modified electrode. *Analytica Chimica Acta* **2020**, *1100*, 232-239.
21. Tian, Y.; Mou, Y.; Zhang, W.; Sun, Z.; Yin, Y.; Han, L.; Chen, D.; Guo, Y.; Sun, X.; Li, F*., et al.* A fluorescence and colorimetric dual-mode aptasensor for kanamycin detection. *Biosensors and Bioelectronics* **2025**, *268*.
22. Xu, Y.; Wen, Z.; Wang, T.; Zhang, M.; Ding, C.; Guo, Y.; Jiang, D.; Wang, K. Ternary z-scheme heterojunction of bi spr-promoted bivo4/g-c3n4 with effectively boosted photoelectrochemical activity for constructing oxytetracycline aptasensor. *Biosensors and Bioelectronics* **2020**, *166*.
23. Li, L.; Li, J.; Wang, S.; Dong, Y. Dual-mode crispr/cas12a-assisted fluorescent and lateral flow aptasensor based on a newly truncated aptamer for fumonisin b1 detection. *International Journal of Biological Macromolecules* **2025**, *298*.
24. Tang, J.; Kou, Q.; Chen, X.; Wang, Y.; Yang, L.; Wen, X.; Zheng, X.; Yan, X.; Le, T. A novel fluorescent aptasensor based on mesoporous silica nanoparticles for the selective detection of sulfadiazine in edible tissue. *Arabian Journal of Chemistry* **2022**, *15*.
25. Ma, K.; Li, X.; Xu, B.; Tian, W. Label-free bioassay with graphene oxide-based fluorescent aptasensors: A review. *Analytica Chimica Acta* **2021**, *1188*.
26. Tian, J.; Wei, W.; Wang, J.; Ji, S.; Chen, G.; Lu, J. Fluorescence resonance energy transfer aptasensor between nanoceria and graphene quantum dots for the determination of ochratoxin a. *Analytica Chimica Acta* **2018**, *1000*, 265-272.
27. Wu, Y.Y.; Huang, P.; Wu, F.Y. A label-free colorimetric aptasensor based on controllable aggregation of aunps for the detection of multiplex antibiotics. *Food Chem* **2020**, *304*, 125377.
28. Chen, C.; Feng, S.; Zhou, M.; Ji, C.; Que, L.; Wang, W. Development of a structure-switching aptamer-based nanosensor for salicylic acid detection. *Biosensors and Bioelectronics* **2019**, *140*.
29. Youn, H.; Lee, K.; Her, J.; Jeon, J.; Mok, J.; Therefore, J.-i.; Shin, S.; Ban, C. Aptasensor for multiplex detection of antibiotics based on fret strategy combined with aptamer/graphene oxide complex. *Scientific Reports* **2019**, *9*.
30. Kou, Q.; Wu, P.; Sun, Q.; Li, C.; Zhang, L.; Shi, H.; Wu, J.; Wang, Y.; Yan, X.; Le, T. Selection and truncation of aptamers for ultrasensitive detection of sulfamethazine using a fluorescent biosensor based on graphene oxide. *Anal Bioanal Chem* **2021**, *413*, 901-909.
31. Zhang, X.; Gao, Y.; Deng, B.; Hu, B.; Zhao, L.; Guo, H.; Yang, C.; Ma, Z.; Sun, M.; Jiao, B*., et al.* Selection, characterization, and optimization of DNA aptamers against challenging marine biotoxin gymnodimine-a for biosensing application. *Toxins* **2022**, *14*.
32. Yu, H.; Pan, C.; Zhu, J.; Shen, G.; Deng, Y.; Xie, X.; Geng, X.; Wang, L. Selection and identification of a DNA aptamer for fluorescent detection of netilmicin. *Talanta* **2022**, *250*.
33. Zhang, Y., Xiong, Y. & Xiao, Y. 3dDNA: A Computational Method of Building DNA 3D Structures. *Molecules* **27**, 5936 (2022).

34. Maier, J. A. *et al.* ff14SB: Improving the Accuracy of Protein Side Chain and Backbone Parameters from ff99SB. *J. Chem. Theory Comput.* **11**, 3696–3713 (2015).
35. Valdés-Tresanco, M. S., Valdés-Tresanco, M. E., Valiente, P. A. & Moreno, E. gmx_MMPBSA: A New Tool to Perform End-State Free Energy Calculations with GROMACS. *J. Chem. Theory Comput.* **17**, 6281–6291 (2021).
36. Van Der Spoel, D. *et al.* GROMACS: Fast, flexible, and free. *J Comput Chem* **26**, 1701–1718 (2005).
37. Ivani, I. *et al.* Parmbsc1: a refined force field for DNA simulations. *Nat Methods* **13**, 55–58 (2016).
38. Bussi, G., Donadio, D. & Parrinello, M. Canonical sampling through velocity rescaling. *The Journal of Chemical Physics* **126**, 014101 (2007).
39. Bernetti, M. & Bussi, G. Pressure control using stochastic cell rescaling. *The Journal of Chemical Physics* **153**, 114107 (2020).
40. Nguyen, H., Roe, D. R. & Simmerling, C. Improved Generalized Born Solvent Model Parameters for Protein Simulations. *J. Chem. Theory Comput.* **9**, 2020–2034 (2013).
41. Aslam, M., Ali, S., Ahmad, K., & Danishuddin. Progress in Electrode Materials for the Detection of Nitrofurazone and Nitrofurantoin. *Biosensors* **15**, 482 (2025).

Tables

Tables are available in the Supplementary Files section.

Figures

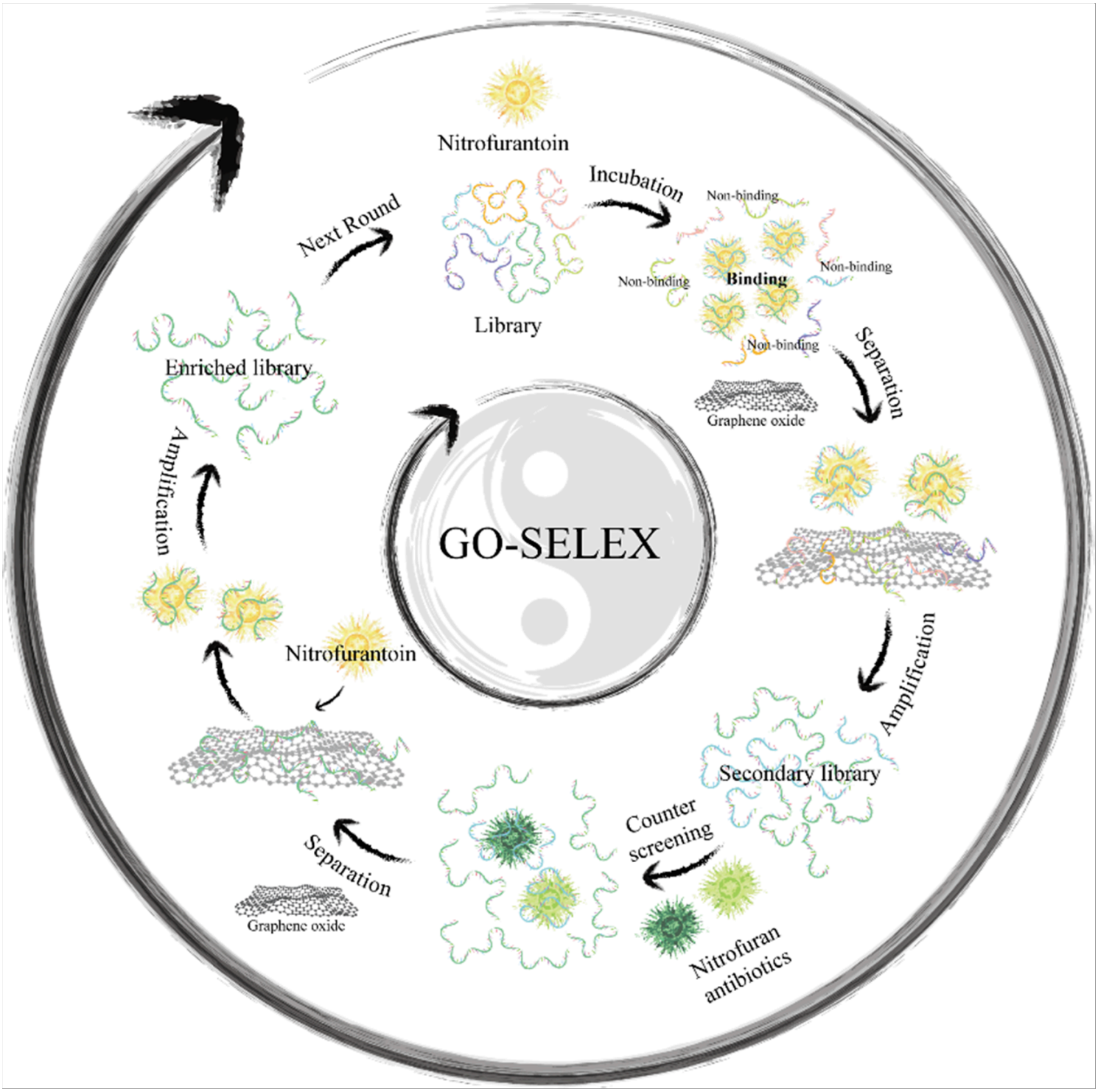


Figure 1

Schematic diagram of the GO-SELEX screening for NFT aptamers.

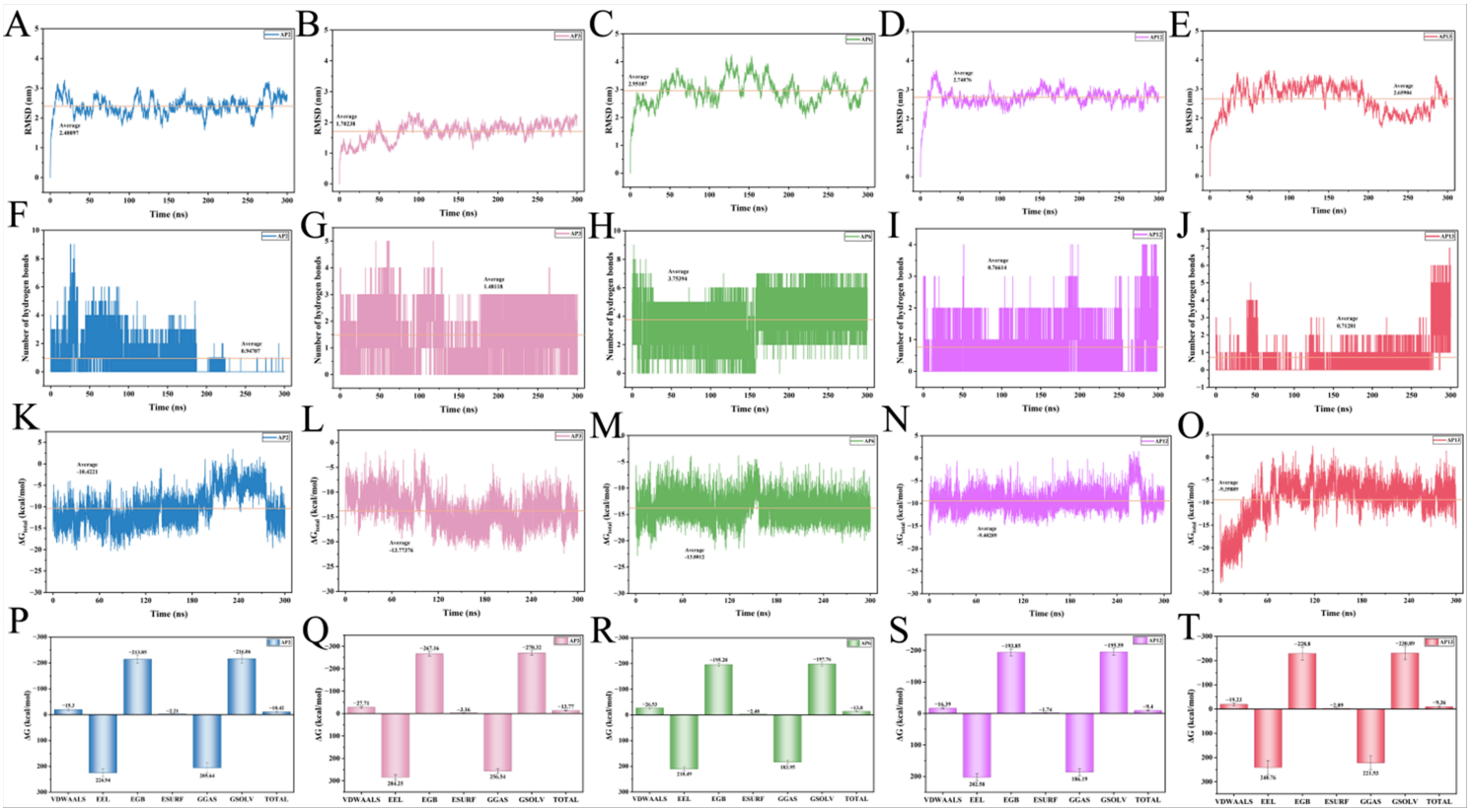


Figure 2

Dynamic stability and binding free energy analysis of different candidate aptamers interacting with NFT. (A–E) RMSD profiles of aptamer–NFT complexes during molecular dynamics simulations. (F–J) Temporal evolution of the hydrogen bonds formed between the aptamers and NFT. (K–O) Binding free energy (ΔG) profiles of the aptamer–NFT complex obtained from MD trajectories. (P–T) Decomposition of the binding free energy into different energy components for each aptamer–NFT complex.

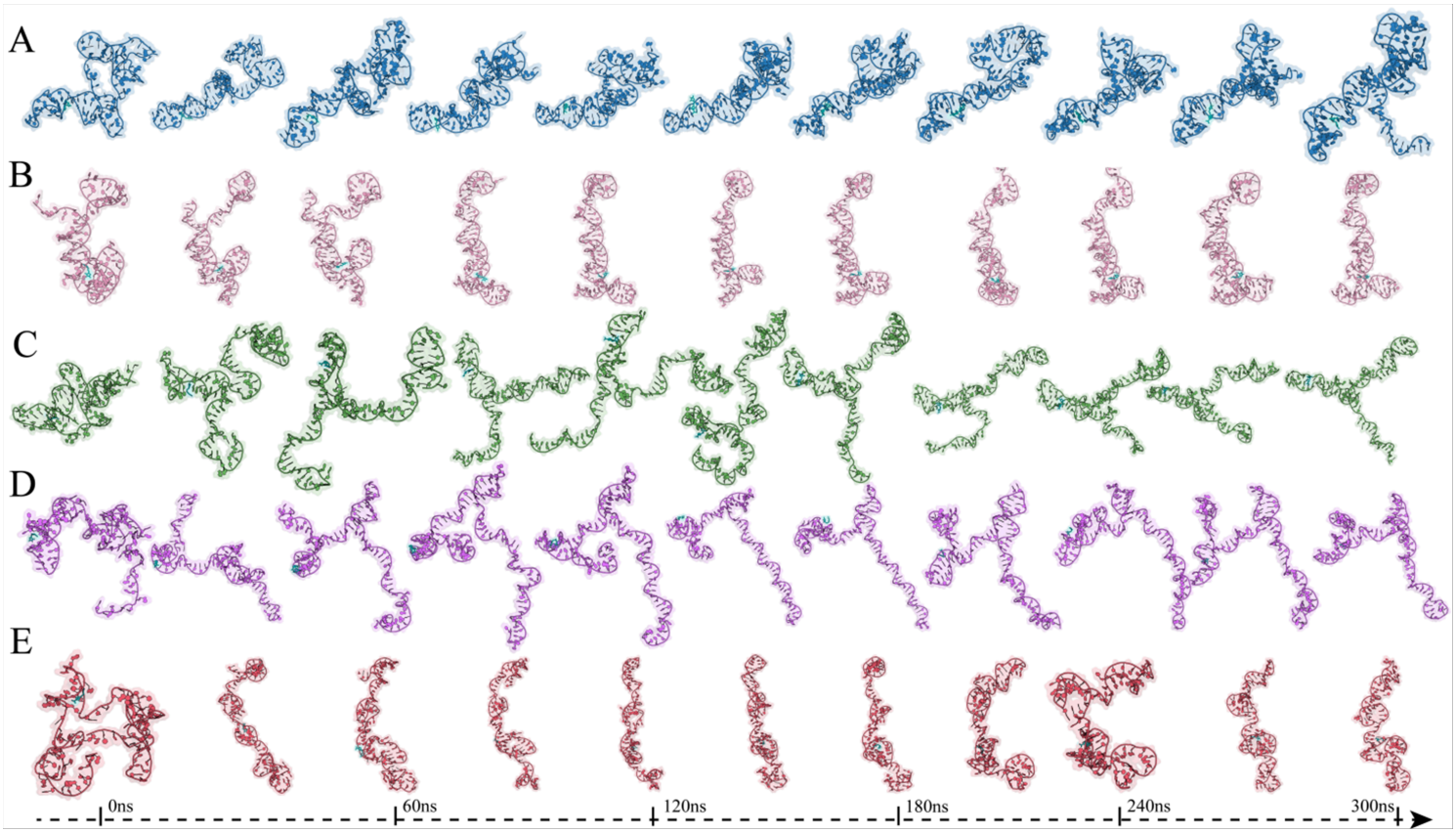


Figure 3

Visualization of the complexes formed between different aptamers and NFT. A total of 11 representative conformations were extracted from the 300-ns molecular dynamics trajectories at 15-ns intervals (including the initial structure at 0 ns). (Note: different aptamers are shown in distinct colors, while NFT is uniformly represented in light blue.).

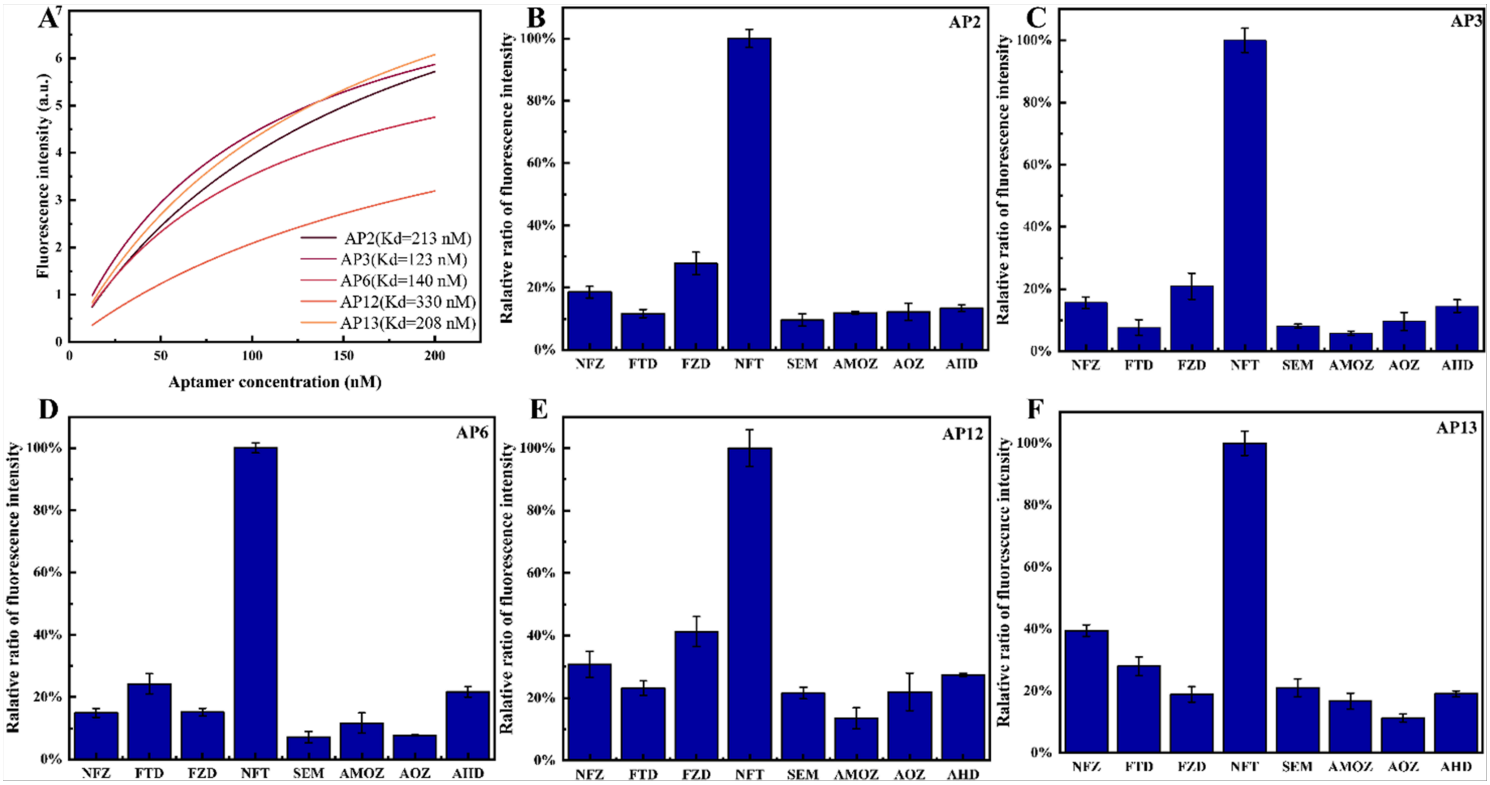


Figure 4

Affinity and specificity of NFT to five candidate aptamers. (A) The affinity of the candidate sequence to NFT was determined by nonlinear fitting; (B), (C), (D), (E), (F) NFT to five candidate sequence specificity tests.

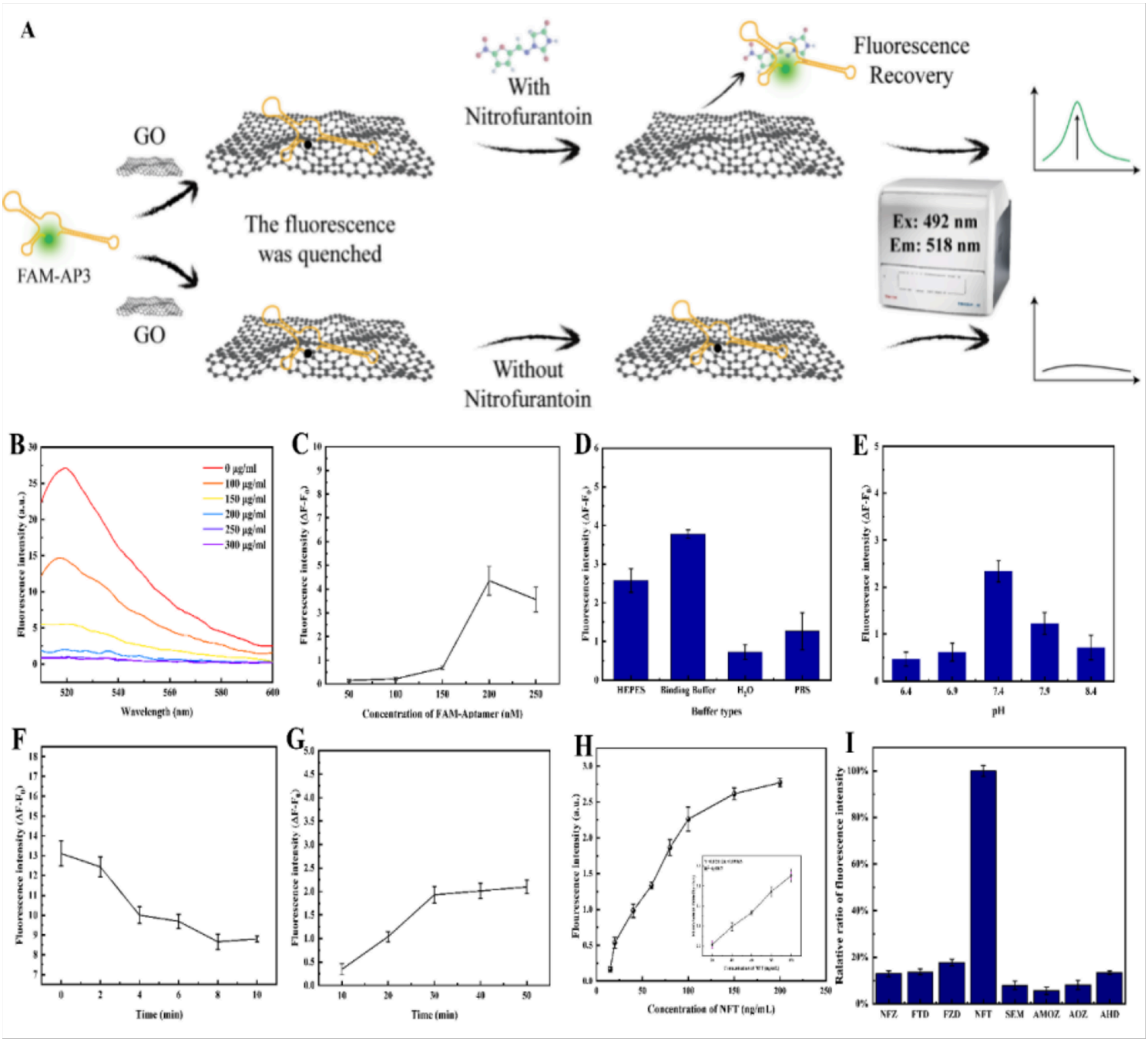


Figure 5

(A) Principle of sensor detection, (B) GO concentration, (C) aptamer concentration, (D) sensor buffer, (E) sensor pH, (F) NFT incubation time with AP3, (H) GO quenching time, and (I) standard curve.

Supplementary Files

This is a list of supplementary files associated with this preprint. Click to download.

- Table1.docx
- Table2.docx

- Supplementarymaterial.docx